New artificial life model for image enhancement

Alex F. de Araujo[1], Christos E. Constantinou[2] and João Manuel R. S. Tavares[1]

[1] Instituto de Engenharia Mecânica e Gestão Industrial, Faculdade de Engenharia, Universidade do Porto, R. Dr Roberto Frias s/n, 4200-465 - Porto, PORTUGAL.

[2] Department of Urology, School of Medicine Stanford University, Stanford, CA, USA.

Corresponding author:

Prof. João Manuel R. S. Tavares

Faculdade de Engenharia da Universidade do Porto (FEUP)

Departamento de Engenharia Mecânica (DEMec)

Rua Dr. Roberto Frias, s/n, 4200-465 PORTO - PORTUGAL

Tel: +315 22 5081487, Fax: +315 22 5081445

Email: tavares@fe.up.pt,

Url: www.fe.up.pt/~tavares

New artificial life model for image enhancement

Abstract

In this work, a method to enhance images based on a new artificial life model is presented. The model is inspired on the behaviour of a herbivore organism, when this organism is in a certain environment and selects its food. This organism travels through the image iteratively, selecting the more suitable food and eating parts of it in each iteration. The path that the organism travels through in the image is defined by a priori knowledge about the environment and how it should move in it. Here, we modeled the control and perception centers of the organism, as well as the simulation of its actions and effects on the environment. To demonstrate the efficiency of our method quantitative and qualitative results of the enhancement of synthetic and real images with low contrast and different levels of noise are presented. Obtained results confirm the ability of the new artificial life model for improving the contrast of the objects in the input images.

Keywords: Image Processing; Image Enhancement; Artificial Intelligence; Artificial Life Model.

1. Introduction

The acquisition, transmission and compression process of the images can damage them, making it difficult, for example, to locate and extract information of the represented objects. Image enhancement techniques have been developed to soften the effect of this damage. These techniques aim to improve the quality of the images and the contrast between the represented objects, highlighting their most significant features and improving the visual perception of relevant features. Moreover, they allow the images to be represented more appropriately for further analysis by computational methods. There are many factors that can contribute to the loss of contrast, such as

loss of focus, noise presence, reflexes, shadows and insufficient illumination of the environment during the image acquisition process [Kao et al., 2010]. The enhancement of degraded images can be improved using different techniques that can be divided into techniques based on spatial domain, the ones that manipulate directly the pixels in the damaged image, and the techniques based on the frequency domain, that work with the image frequency information, generally obtained by Fourier and Wavelets transforms [Hanmandlu et al., 2003, Trifas et al., 2006].

The image enhancement techniques applied on the spatial domain are widely used and try to manipulate directly the image pixels, performing computational operations on these pixels based on their values. For example, considering an image in gray scale, where the intensities can have values from 0 (zero) to 255, we verify that the intensities of the original image use only a reduced range of these values. So, the enhancement methods on the spatial domain try to redistribute the intensities in a way that they can use a wider range of values, improving the perception of the different objects in the image. Some of the traditional techniques applied on the spatial domain are based in the histogram equalization, normalization, quadratic enhancement, square rooted enhancement and logarithmic enhancement [Gonzalez and Woods, 2006].

The enhancement in the frequency domain has its techniques based on the convolution theorem and can be interpreted as an enhancement extension in the spatial domain, with its operations applied to the image frequencies, usually obtained by the application of a transform, as the Fourier Transform. After the frequencies manipulation, an inverse transform is applied so that the image can be represented again in the spatial domain. This kind of enhancement method is generally obtained through filtering techniques, as the high-pass filter [Gonzalez and Woods, 2006].

Recent studies have been adopting models based on artificial life to process tasks of the computational image processing and analysis obtaining effective results. Examples include brain segmentation in magnetic resonance images [McInerney et al., 2002, Farag et al., 2007, Feng et al., 2008, Prasad et al., 2011a, Prasad et al., 2011b], and features extraction and classification from medical images [Srinivasan and Sundaram, 2013]. The use of these artificial life models, better

known in computational image processing, tries to make a deformable “living” model provided with a "primitive brain" capable of making decisions in search of the best results in the segmentation process.

The objective of this paper is to present a new method based on artificial life to image enhancement based on the modelling of an organism, in particular, its control and perception centers. On the contrary of what is common in image segmentation processes using artificial life models, our model is not inspired in the organism’s shape, that is, the geometry of the organism’s body, but in its behavior when it is located in a certain environment and performs the food selection process. With the proposed enhancement method, it is intended to enhance images with low contrast and images affected by noise interference, highlighting the transitions between presented objects, and at the same time avoiding enhancing the noise that affects the original image quality. The results of the proposed enhancement method using the developed model allow us to conclude that this method is promising, being capable of considerably improving the visual perception and the quality of the affected images. Another contribution of this work is the innovating utilization of artificial life models as enhancement image techniques.

This paper is organized as follows: in the next section, a review about existing artificial life models is presented. In section 3, the proposed model is described. Experimental results are presented and discussed in section 4, following the obtained conclusions and suggestions for future work.

2. Review about methods based on Artificial Life

The studies related with computational image processing and analysis try to develop methods capable of manipulating complex images with different features, in an efficient, robust and reliable way. Various computational methods to different tasks can be found in the literature, such as for noise removal [Chen et al., 2010, Cao et al., 2011, Zhang et al., 2010a], enhancement [Cheng and Xu, 2000, Cheng et al., 2003, Lai et al., 2012, Cho and Bui, 2014], segmentation [Xue et al., 2003,

Nomura et al., 2005, Ma et al., 2010a], tracking [Pinho and Tavares, 2009, Nguyen and Ranganath, 2012], registration [Oliveira et al., 2011, Oliveira et al., 2010] and recognition [Papa et al., 2012]. Besides the diverse tasks that can be made by these methods, many techniques have been used, as Genetic Algorithms [Wang and Tan, 2011, Hashemi et al., 2010, Yi Kim and Jung, 2005], Artificial Neural Networks [Petersen et al., 2002, Shkvarko et al., 2011], Active Contours [Ghita and Whelan, 2010, Ma et al., 2010b], Region Growing [Fan et al., 2005, Peter et al., 2008], models based on differential equations and finite elements [Chao and Tsai, 2010, Yu et al., 2010].

A research field based on artificial life has emerged in the computer graphics area for modeling animation behavior and the evolution of plants and animals [Kim and Cho, 2006]. This investigation area has also formed the basis for new researches in computational image processing and analysis [McInerney et al., 2002, Farag et al., 2007, Feng et al., 2008, Prasad et al., 2011a, Prasad et al., 2011b, Osuna-Enciso et al., 2013, Horng, 2011], forming the methods called image processing methods based on artificial life models.

The artificial life models address the diverse biological processes that characterize the live species in the attempt to overcome the problems found in the image processing, such as the complexity of the represented objects and low contrast between them and the rest of the represented scene. The majority of the artificial models used in this area apply techniques based in physical and geometrical principles, aiming to make the used deformable models [Ma et al., 2010b] more flexible and capable of performing a better image exploitation, using a priori knowledge of the area associated with the images, and analyzing better the neighborhood of the active model used to control the deformation in a more adequate and robust way. Making an analogy with the artificial life systems, the geometry of the deformable model is generally considered as being an "organism" (a worm), that keeps changing according to the available priori knowledge, associated with the information that its sensorial organs return while the organism changes its shape and moves through the image (or environment). Despite being the most common utilization of the artificial models in image processing, there are many biological processes that can be used as basis for the same

models, such as growing, natural selection, evolution, locomotion and learning [Kim and Cho, 2006, McInerney et al., 2002].

Another important issue is that the models based on artificial animal life are more relevant to the image processing techniques, because they present bodies with motor and sensorial organs, and mainly a brain with learning (cognitive system), perception and behavioral centers [McInerney et al., 2002, Horng, 2011]. The motor center coordinates the muscular actions to perform specific actions, as locomotion and the control of the sensorial center. This last one is used so that the artificial organism acquires information about what happens around it and sends this information to the cognitive center, which is going to decide which actions must be performed to obtain best results according to each situation. The perception center is the part of the brain that allows the organism to have its sensors trained, being formed by mechanisms that allow it to acquire and understand sensorial information about the environment that surrounds it. This behavior is useful to perceive the modifications that occur during the processing, since the individual actions can have significant changes in the environment. The learning center allows the individual to learn how to control all his organs and his behavior through practice. The bahavioral center has the routines with the actions that the individual must perform, considering their perception. For the creation of an artificial life model, the work-tasks pyramid shown in Figure 1 is usually followed.

(Insert Figure 1 about here)

Observing the pyramid in Figure 1, from bottom-up, there is the organism's geometric modeling in its base. In this layer, the organism's type is defined, as well as its appearance and geometric morphology. In the second layer, there is the physical modeling where the biomechanical principles are modeled for simulation and formation of the biological tissues, such as muscles. The next layer incorporates the motor control routines, which are responsible for stimulating the muscle actuators

to allow the locomotion movements. In the fourth layer, there is the behaviour and perception modeling, with an important part, for example, in detecting and navigating between obstacles. And on the top of the pyramid, the cognitive layer, which is responsible for controlling the acquired knowledge by the organism during the learning process, as well as the planning of the actions to be performed with some level of intelligence.

3. Proposed Model

The computational image processing based on artificial life models uses an analogy between biological processes from certain organisms and the desired operations to do on the images being processed. One of the objectives of these models is to automate the applied computational methods, making them more robust, efficient and automated to deal with the existing variations in the involved image set. The organisms used in the models have features that deserve highlighting: they are endowed with a prior knowledge about some features of the environment, namely from the scene, in which they are found; they have sensors that operate in making decisions about the actions to be performed during processing; they have a set of actuators that in association with a knowledge system, allows the organism to adapt to the environment according to the collected data from the sensors.

Some models based on artificial life, such as the ones based on worm, called deformable organisms, have been successfully used in the image segmentation; as in, for example, [McInerney et al., 2002, Farag et al., 2007, Prasad et al., 2011b]. Usually these models have an analogy to worms, considering their great flexibility and their subsequent facility to deformation. Thus, each organism has a "skeleton" defined to describe its initial shape. When the organism is placed in an image, it starts a search for a compatible region with the geometry of its skeleton and with the a priori knowledge that it has about the input scene. When a compatible object is found, a set of sensors and

actuators start to work, deforming the worm’s "skeleton" evolving this “skeleton” in order to fully enclose the object’s region in the input image.

Although this technique of artificial intelligence has been wide used for image segmentation with considerably success, it has not been so common for image enhancement. Hence, we extend it use to enhance the contrast of images by proposing a new artificial life model. The adopted model is not based on analogy with the organism’s body shape, but on the behaviour of a herbivore organism when it is in a specific environment and performs the process of selection of its food. The organism’s body shape was not considered in this approach because what matters here is the effect that the behaviour of this organism produces in the environment, and the shape of its body has no direct influence on the operations considered in this work. In Figure 2, there is the flow diagram of the proposed method, with the steps of the method described in detail in the following sections.

(Insert Figure 2 about here)

3.1. Model Description

The low contrast images problem can be reduced using computational methods for image enhancement, making the difference between different objects more enhanced, allowing us to obtain better results in the later stages of image processing and analysis, such as segmentation and features extraction. Considering a grayscale image, it is desired that the pixels with low and high intensities are represented so that their intensities are as distinct as possible. Based on this principle, a good enhancement method in the spatial domain is the one able to verify all pixels of an original image, and recalculate their intensities taking into account the neighbours so that the intensity differences between the pixels belonging to neighbouring and distinct regions is increased. Thus, the model based on artificial life used in the proposed image enhancement method was inspired by the behaviour of the herbivorous organisms when they are in a specific environment and perform

the selection process of its food. To this end, it was considered a natural pasture as environment. These considerations have resulted from the observation that while feeding on a natural pasture, these organisms make a selection of the food, setting a "priority order" of the food to be eaten first. If we consider an area composed by a single type of food with different heights, there is a tendency that the smaller food will be eaten first. Usually this happens because the smaller parts are smoother and more nutritious than the bigger ones. Furthermore, the organism is not fixed in a single point until it eats all of the food available there. In general, it is always moving in the environment while feeding itself, guided by its cognitive system using the information collected about the food around it. Thus, the difference between the small and big foods present in a given environment tends to become more evident, at the same way as it is desired in the image enhancement operation. In the built model, the organism moves iteratively on the image until a threshold for the height of the food is reached.

3.2. Modeling the control center

The control center has been modeled from the movement operations of the organism, and reduces the height of the food as a result of the eating process performed by organism. Two control operations are defined in this step: moving and reducing the height ("eat"). The movement consists in moving the organism from one point to another one on the image, avoiding passing through the same point more than one time at the same iteration. In each iteration, all pixels of the image are visited and their intensities are recalculated. To simulate how the organism feeds, the intensity of each point is reduced by considering the following assumptions: usually the organism eats a bit of food that is in the region where it is, but it does not always eat all the food at the same time; the smaller foods are fresher and more nutritious, and they have priority to be consumed. These assumptions are part of the a priori knowledge set that the organism has about their actions and the environment. So, considering a local analysis on the image, the smaller its current value, the bigger

the reduction of the intensity value of each pixel; i.e., in a very bright pixel a small reduction occurs while in darker pixels a greater reduction, in proportion to its size, is performed in each iteration. To model this behavior, we adopted the following rational function:

$$f(x) = \frac{kx}{x^2 + k}, \quad (1)$$

where $x = 0, 1, ..., 255$ is the possible intensity values for pixels in the 8-bits images, and *k* is a positive constant used to control how much of the food height should be reduced at each iteration. The higher the value of *k*, the faster the food is reduced and less time is spent to reach the stop criterion. However, very high values for *k* cause similar regions to merge quickly, and distinct objects may be wrongly joined. On the other hand, if its value is too low, the growth of the food can be greater than the amount that is eaten, so the different objects represented in the image can be joined to the image foreground. As the intensities of the pixels in the input images range from 0 to 255, *k* was defined as equal to the maximum possible value, i.e., $k = 255$. As such, if the intensity of a pixel is 0 (*zero*), the reduction is also 0 (*zero*), but if the intensity is 1 (one), then the reduction is almost equal to the total height associated to the pixel. This behavior is repeated for all pixels with low intensity, and for pixels with high values, the reduction is smaller. It should be noted that, in the images considered in this work, the pixels belonging to the regions of interest are almost black. For this reason, it was considered that the best “food” (i.e., the darkest pixels) has the maximum possible height, which was experimentally considered as equal to 10% of the maximum available height.

The function of Equation 1 generates a curve which shows a more significant loss for the pixels with smaller intensity, while those with bigger intensities are less affected, Figure 3. Thus, the darkest pixels tend to darken faster than the lighter ones, increasing the difference between them and, consequently, improving the enhancement of the image associated area.

(Insert Figure 3 about here)

3.3. Modeling the perception center

The perception center was modeled according to the a priori knowledge of the organism's behaviour, considering the information about the neighbourhood acquired by the organism. The perception center will act primarily to receive the height information of the neighboring points of the organism; i.e., the intensity level, and which points have been visited in a given iteration. This information is important to choose the way for the organism to go. To determine how to move in the environment, all 8 (eight) pixels neighboring the pixel occupied by the organism are visited, and at the same time that the intensity of the visited pixel is reduced, the organism stores the coordinates of the pixel with smaller intensity, which is added to its path at the end of the visit to the neighboring pixels. In addition, the visited pixels are marked as visited, being released for further visits after the end of the current iteration. This operation allows the organism to walk in a coordinated way in the image, following the darker regions. However, it may happen that the organism is isolated in a pixel whose all the neighbors have already been visited. In this case, the organism carries out a search for the nearest pixel that has not yet been visited and continues processing. This search for the nearest pixel ensures that all pixels on the image are visited, and have their values updated at each iteration.

3.4. Effects of the organism’s actions in the environment

The organism walking process in the environment following the points with best food generates a secondary effect, which is the damage to the bigger foods during the movement process, since the organism moves over them. This effect is much common because the big foods are less flexible and are frequently broken when they are pressed, and the broken parts are usually discarded because when food is damaged, it loses its nutritive capability, and it will hardly be consumed by the organism.

Another interesting effect that happens with the adopted model is a consequence of the time that the organism needs to eat all the food available. Under the considered conditions in the used analogy, many days are usually needed for this process to be performed. So, as the food is a natural herb, the pieces not yet fully eaten tend to grow as time goes by. However, very big foods and even those small ones tend to be broken rather than grow, and the high ones break due to their low flexibility, as already previously explained, and the small ones do too because they are young and have low resistance. Thus, only those foods with middle height usually grow effectively. So to simulate these effects the function of Equation 2 was adopted, because this one represents an undulating curve, ranging from the approximate range of $[-y_1, y_2]$, where y_1 and y_2 belong to the set of real numbers, as can be seen from the curve of Figure 4. In that curve, the values y_1 and y_2 are the smallest and the biggest values along the Y-axis, respectively. This curve allows the performance of an approximate simulation of the degrading operations of the big and small foods and the growth of the intermediate foods according to the course of time:

$$f(x_i) = \frac{\sin\left(\frac{2}{3}\sqrt{\frac{x_i\pi}{180}} + \frac{\pi}{4}\right)}{\sqrt{\pi}\sqrt[4]{\frac{x_i\pi}{180}}}. \quad (2)$$

(Insert Figure 4 about here)

3.5 Stopping Criterion

In the implemented method, we tried to integrate an automatic stopping criterion based on a threshold defined from the height of the food present in the environment. For this purpose, while the organism moves in the environment, the heights of the foods are summed and compared with the sum of the heights in the input image, and the processing is finished as soon as at least 30% of the

height of all foods has been eaten. This threshold was defined experimentally for the images to be studied.

4. Results and Discussion

To test the efficiency of the proposed model, it was necessary to take images where it is possible to quantitatively measure the loss of contrast in the output image when compared with the ideal image, as well as the restoration rate obtained from the application of the proposed enhancement method. For this purpose, 8 images were used for testing, where 4 grayscale images were synthetically created and the other 4 were real ones, including the traditional images "Lena" and "Cameramen". After that, each image was damaged twice, resulting in 16 grayscale images with changed contrast. Both reduction contrast processes were applied over the original images, and in each of them a Gaussian noise was added with intensity equal to 0.3, and in one of these reduction contrast processes a circular median filter was applied with radius equal to 2 for blurring the image before applying the noise. The results of the image enhancement obtained from the images with the contrast affected were visually and statistically analysed based on the analysis of the indexes returned by PSNR (Peak Signal Noise Ratio), SSIM (Structutal Similarity) and Detail Variance and Background variance (DV-BV) metrics. The PSNR and SSIM indexes were calculated comparing the original image and the images resulting from the controlled degradation process. In addition, we analyzed the profile of a random line of the images, and compared the proposed method with other enhancement methods traditionally used in the spatial domain: normalization, histogram equalization, square enhancement, square root enhancement and logarithmic enhancement methods [Gonzalez and Woods, 2006].

4.1. Adopted evaluation metrics

Generally, the comparison between two images is a natural task for the human visual system, but the realization of this same task for a computer system is more complex and not so natural. However, there are many studies attempting to provide techniques able to compare images, including techniques to statistically compare the performance of image processing methods [Wang et al., 2004, Ramponi et al., 1996].

4.1.1 Analysis based on error

The indexes of comparison based on error try to estimate the perceived error between the processed image and the original image to quantify the image degradation. The techniques of this category have as their main disadvantage the fact that they can fail in cases where translations in the images happen. For example, similar images where one of the objects has been displaced can be classified as distinct by this process. Moreover, these indexes perform the comparison based on the variation of the intensities of the pixels in the images, and images with different types of distortion can have similar indexes [Wang et al., 2004]. Despite of that, the indexes based on error are often used to compare the quality of image enhancement [Hashemi et al., 2010, Shkvarko et al., 2011, Ghita and Whelan, 2010] and image smoothing [Chen et al., 2010, Jin and Yang, 2011] methods, due to their simplicity and the fact that these images are usually affected by a few displacements during the computational processing.

Some of the most known indexes based on error are the PSNR (Peak Signal Noise Ratio), RMS (Root Mean Square), MSE (Mean Squared Error) and ReErr (Relative Error) [Wang et al., 2002]. However, the most commonly used to analyze the performance of the restoration and enhancement methods is the PSNR, which attempts to calculate the relationship between the highest possible force strength of a signal (in the case of the image it is the highest intensity value) and its strength affected by noise [Dash et al., 2011, Yang et al., 2009]. In this case, the PSNR is represented in

function to a logarithmic scale on the base 10 (decibel), because some signals have a very high value. The PSNR can be calculated from the MSE, which can be defined as:

$$MSE = \frac{1}{m\,n} \sum_{i=0}^{m-1} \sum_{j=1}^{n-1} \left[I(i,j) - I_r(i,j) \right]^2 , \qquad (3)$$

where m and n are the dimensions of the input image, I is the original image, and I_r is the affected image by processing or by any artifact.

From the MSE index, the PSNR can be calculated as follows:

$$PSNR = 10 \log_{10} \left(\frac{MAX_I^2}{MSE} \right), \qquad (4)$$

where MAX_I is the maximum value that a pixel can be. To the grayscale images represented by 8 bits, for example, $MAX_I = 255$. During the interpretation of the PSNR index, the higher its value, the more similar are the two compared images. It is important to note that for identical images, the MSE index value will be zero, and thus the PSNR is undefined.

4.1.2 Analysis based on structural information

This approach attempts to note the changes in the structural information of the image to quantify the occurred degradation. The analysis of the structural information assumes that the human vision system is adapted for extracting structural information from what is seen, searching for changes in these structures to detect changes and consequently, possible degradation generated by some process [Wang et al., 2002]. The SSIM index (Structutal Similarity) is an index of this class most often used to analyze the quality of computational methods for image processing [Zhang et al., 2010b, Chen et al., 2010].

The SSIM index was proposed by Wang and colleagues [Wang et al., 2004] in an attempt to avoid that the images with very different visual qualities have the same index, as can happen in the

indexes based on error. This index is calculated based on three components of comparison: luminance, contrast and image structure. The first parameter is calculated from the average intensity of the signal, in this case the input image. The contrast is calculated from the standard deviation, and the structure parameter is computed from the normalized image using the standard deviation of the same image. So, the SSIM index can be obtained using the equation:

$$SSIM(x,y) = l(x,y)^{\alpha} . c(x,y)^{\beta} . s(x,y)^{\gamma}, \quad (5)$$

where, $\alpha > 0$, $\beta > 0$ and $\gamma > 0$ are constant parameters used to define the weight of each component in the final index. The component l refers to the luminance, c to the contrast and s to the structure. The three components are relatively independent, and changes in one of them do not affect the other ones. In [Wang et al., 2004] a more detailed analysis of each component is presented, showing in detail how they are calculated. The SSIM value shows an index for each pixel of the image and, to make its use more practical, it is common to use a mean SSIM index, also called MSSIM, which is calculated from the average of the elements obtained from SSIM. For equal images, this index is equal to 1 (one positive), being reduced as the images differ, reaching the value -1 (negative one) for two images exactly opposite (one image is the negative of the other one).

4.1.3 Detail Variance and Background Variance values

The Detail Variance (DV) and Background variance (BV) values are used to give indications about the level of enhancement in an image, without necessarily using the other image as a benchmark. These values are calculated from the local variance of the *n* neighbors of all image pixels, creating a matrix of variances in a first step. Afterwards, each pixel is classified into two classes: the variance of each pixel is compared to a threshold, and if it is greater than the threshold value, the pixel is classified as belonging to the image foreground, otherwise the pixel belongs to the image background.

After classifying all pixels of the image, the mean variance of the pixels belonging to two classes are calculated, and respectively called DV and BV. To check the level of enhancement applied to the image, these two values are analyzed as follows: if the DV index of the processed image increases when it is compared to the DV index of the input image, while the BV value suffers a little change, it is considered that the image was efficiently enhanced. In this work, we adopted a neighborhood of $n \times n$ neighbors, and the threshold was calculated using the Otsu method [Osuna-Enciso et al., 2013].

4.2. Experimental Tests

In Figures 5, 6 and 7, the results obtained by applying the square root enhancement method are presented (c); quadratic enhancement method (d); logarithmic enhancement method (e); normalization method (f); histogram equalization method (g); and proposed enhancement method (h), on the input image with reduced contrast (b). In each figure, the image (a) represents the original image and the images together with the symbol (-) represent the difference between the processed images and their respective original images, for example, the image (b-) is the difference between the images (b) and (a), (c-) is the difference between the images (c) and (a), and so on. Note in these figures that the proposed method (figures 5h, 6h and 7h) allowed to enhance properly the objects represented in the input images (figures 5b, 6b and 7b, respectively), restoring the transition details between such objects, as can be seen with more accuracy in image (h) of Figure 5. In addition, our method allowed to maintain the transitions in the areas with linear transitions of the gray levels, as noted in image (h) of Figure 6. Analyzing the difference between the processed images (b-, c-, d-, and f-) and their respective original images, it is possible to note that the proposed method returned images more similar to their respective original images (figures 5a, 6a and 7a). Note that the difference between two identical images generates an image in black (image

a-), i.e., the darker the image resulting from the difference, the more the processed image is similar to the original image, indicating a better result.

(Insert Figure 5 about here)

(Insert Figure 6 about here)

(Insert Figure 7 about here)

In Figure 8, the results of the same enhancement methods applied in 4 real images are presented, including images "Lena" and "Cameramen" with contrast affected by the addition of synthetic Gaussian noise. The respective PSNR and SSIM indexes for the 4 images are presented in Tables 1 and 2, in lines 13, 14, 15 and 16, respectively. It is possible to note from the analysis of the indexes and the images of Figure 8 that the proposed method obtained promising results, being able to restore the contrast in the input images.

(Insert Figure 8 about here)

To complement the comparison of the results, a quantitative analysis of the results was made using the PSNR and SSIM indexes. These indexes were obtained from the comparison between the original images and their respective images resulting from the application of the enhancement methods, Tables 1 and 2. In these tables, the values obtained for the synthetic images shown in Figs. 5–7 are indicated in bold.

(Insert Table 1 about here)

(Insert Table 2 about here)

The PSNR index allows the performance of an analysis based on error, showing the ability of our enhancement method to restore the information intensity of the pixels of the degraded image. The PSNR indexes for different methods of enhancement tabulated in Table 1, and plotted in Figure 9 allow us to check the best performance of the proposed method. From the presented graph, it is possible to clearly note that the results of the new method were better for all images from the test set, since the PSNR index had the highest values for this method.

(Insert Figure 9 about here)

The SSIM index shows the ability of the processing method to preserve the structural information of the processed image. The graph of Figure 10 has been plotted from the data presented in Table 2, and together with the analysis of Figure 9, it allows us to conclude that our method was able to enhance the input images, preserving the structural information of the processed images better than the other methods presented in the literature, as indicated by the highest values for the SSIM index.

(Insert Figure 10 about here)

To complement the analysis of the proposed enhancement method, the profile of a line of the original images, affected and resulting from the application of the method was extracted and plotted in the graphs of Figure 11. In this figure, the profiles of a random row of images of the images of

Figures 5, 6 and 7, respectively, are presented. The graph of the line profile for each image has three components: the blue component for the line profile in the original image; the red line for the affected image; and the green one for the image result of the proposed method. The extraction of the line profile showed that the image affected had the line profile very irregular due to interference caused by damage in the original image with the addition of noise. In addition, the line profile of the image presented in Figure 5 shows the smoothed transition due to the blurring operation. Through the analysis of these graphs, it is clear that the method has greatly approximated the input image to the original image, reducing the smoothing transitions between objects and also reducing the interference caused by noise. This behavior was observed for almost all images studied.

(Insert Figure 11 about here)

Another objective analysis that can be made about the results of the image enhancement methods is through the DV and BV values. In Table 3 the DV and BV values for the 4 images of Figure 8 (Cup, Lena, Cameramen and Parrot) are presented. In the second column of the table, the values of the original images are indicated in bold as are the values that should be approximated after the application of the enhancement methods under comparison. It is possible to note from these data that the proposed enhancement method obtained the best results for three of the four analyzed images (Cup, Lena and Cameramen), returning images with high DV values and BV values close to the respective values in the original image.

(Insert Table 3 about here)

To better visualize the results of this analysis, the points classified as belonging to detail value (DV) of the four images of Figure 8 were marked in black color and the images are presented in Figure

12. Note that the detected details from the images processed by the proposed method (h) are closer to the detail detected from the original images (a) indicating that the proposed method performed a more efficient processing than the other methods tested.

(Insert Figure 12 about here)

In Figure 13, we have the result of the proposed method and the enhancement methods studied in this paper applied in real images. It is observed that the resulting images of the enhancement proposed method allowed a more efficient segmentation of the images, due to the enhancement of the transitions between the inner and the outer regions of the objects. It is noted from the edges extracted by the Chan-Vese method [Chan and Vese, 2001]. In the ultrasound image of the pelvic cavity, it is noted that a greater part of the bladder was detected in the image enhanced by the proposed method (image h). In image "Cameramen", it is also realized that the edges extracted from the image enhanced by the proposed method is more regular, and the objects are better involved. In the image of the skin lesion, an edge with less discontinuity was obtained, even though the lesion was in an area affected by the strong presence of hair.

This work presents a pioneer application of an artificial life model for image enhancement. The results obtained using both synthetic and real images exposed that one advantage of the proposed model is a superior enhancement of the image transitions, making the structures presented from the image background more distinguishable, and the higher preservation of the structural information presented. Another advantage of the model developed is that it is based on the behavior of the organism mimicked instead of being based on the organism morphological characteristics, as happens with the deformable models commonly used in image segmentation. Although the evident advantages, the presented model can still be improved, for example, by integrating more

sophisticated cognitive and sensorial centers that will increase the efficiency and robustness of the enhancement process.

(Insert Figure 13 about here)

Being an iterative method, the proposed method requires a higher computational time than the other methods discussed, Table 4. In that table, the times required to enhance the images "Lena" and "Cameramen" are indicated, both images are in grayscale and with size equal to 256x256 pixels. The tests were performed using a core of an Intel Core i5 processor at 3.2 GHz, 8 GB of RAM and 64-bits bus. The time for each method was obtained by averaging 150 executions, in order to increase the accuracy of the indicated values.

(Insert Table 4 about here)

5. Conclusions

The proposed method for image enhancement in the spatial domain is based in a new artificial life model, which processes the original image using operations based on the pixels' values in order to highlight the intensity differences between neighbour regions. In comparison to other well known enhancement methods presented in the literature, the suggested method showed very promising experimental results.

A quantitative and qualitative analysis of experimental results concluded that the proposed method is able to improve the transitions between the objects presented in degraded images, and got better results than the traditional enhancement methods adopted and compared in this work. In addition, tests on real images, such as ultrasound of the pelvic cavity, "Cameramen" and the image of a skin

lesion, showed that the proposed method is capable of enhancing the transitions between the structures present in these images, increasing, for example, the efficiency of the segmentation methods.

The analysis of the results obtained by the proposed model confirmed that, as in several applications of image segmentation, the artificial life models can accomplish acceptable results in applications of image enhancement, suggesting these models also for the field of computational image processing. The effective image enhancement makes the image segmentation step easier and more accurate as it was demonstrated by using the Chan-Vese segmentation method on enhanced images. Additionally, the characterization and classification of structures from images can be more robust, once these tasks are highly dependent on the quality of the image segmentation step.

Moreover, the experimental results obtained using the proposed image enhancement method allow us to conclude that the new artificial life model is very interesting for ultrasound imaging, once the ultrasound images are commonly affected by artifacts during the acquisition process, and the transitions between the structures presented are attenuated. Hence, the method proposed can effectively contribute for a more successfull ultrasound image processing and analysis by emphasizing the transitions between the structures presented and reducing the artifacts.

In future studies, we intend to integrate the modeling of the cognitive center to the organism of the proposed model, giving it the ability to make smarter and elaborated decisions, as well as add some other control parameters of the environment, such as its relief, which can influence in the way that the organism moves in the enviroment. We also intend to extend the proposed method to improve the enhancement of image sequences using the relationship between consecutive frames.

Furthermore, we want to apply techniques of high performance computing to reduce the computational time of the proposed method, such as parallel computing and processing using multiresolution.

Acknowledgments:

The first author would like to tanks Fundação para a Ciência e Tecnologia (FCT), in Portugal, for his PhD grant with reference SFRH/BD/61983/2009.

This work was partially done in the scope of the project “A novel framework for Supervised Mobile Assessment and Risk Triage of Skin lesions via Non-invasive Screening”, with reference PTDC/BBB-BMD/3088/2012, financially supported by Fundação para a Ciência e a Tecnologia (FCT) in Portugal.

References

[Cao et al., 2011] Cao, Y., Luo, Y., and Yang, S. (2011). Image denoising based on hierarchical markov random field. *Pattern Recognition Letters*, 32(2):368–374.

[Chan and Vese, 2001] Chan, T. and Vese, L. (2001). Active contours without edges. *IEEE Transactions on Image Processing*, 10(2):266 –277.

[Chao and Tsai, 2010] Chao, S.-M. and Tsai, D.-M. (2010). An improved anisotropic diffusion model for detail- and edge-preserving smoothing. *Pattern Recognition Letters*, 31(13):2012–2023.

[Chen et al., 2010] Chen, Q., Sun, Q., and Xia, D. (2010). Homogeneity similarity based image denoising. *Journal of Pattern Recognition*, 43(12):4089–4100.

[Cheng and Xu, 2000] Cheng, H. and Xu, H. (2000). A novel fuzzy logic approach to contrast enhancement. *Pattern Recognition*, 33(5):809–819.

[Cheng et al., 2003] Cheng, H. D., Xue, M., and Shi, X. J. (2003). Contrast enhancement based on a novel homogeneity measurement. *Pattern Recognition*, 36(11):2687–2697.

[Cho and Bui, 2014] Cho, D. and Bui, T. D. (2014). Fast image enhancement in compressed wavelet domain. *Signal Processing*, 98(0):295 – 307.

[Dash et al., 2011] Dash, R., Sa, P. K., and Majhi, B. (2011). Restoration of images corrupted with blur and impulse noise. In *Proceedings the International Conference on Communication, Computing & Security*, volume 1, pages 377–382.

[Fan et al., 2005] Fan, J., Zeng, G., Body, M., and Hacid, M.-S. (2005). Seeded region growing: an extensive and comparative study. *Pattern Recognition Letters*, 26(8):1139–1156.

[Farag et al., 2007] Farag, A. A., Suri, J. S., Micheli-Tzanakou, E., Hamarneh, G., and McIntosh, C. (2007). Deformable organisms for medical image analysis. In *Deformable Models*, Topics in Biomedical Engineering. International Book Series, pages 387–443. Springer New York.

[Feng et al., 2008] Feng, J., Wang, X., and Luo, S. (2008). Medical imaging and informatics. chapter A Worm Model Based on Artificial Life for Automatic Segmentation of Medical Images, pages 35–43. Springer-Verlag.

[Ghita and Whelan, 2010] Ghita, O. and Whelan, P. F. (2010). A new gvf-based image enhancement formulation for use in the presence of mixed noise. *Pattern Recognition*, 43(8):2646–2658.

[Gonzalez and Woods, 2006] Gonzalez, R. C. and Woods, R. E. (2006). *Digital Image Processing (3rd Edition)*. Prentice-Hall, Inc., Upper Saddle River, NJ, USA.

[Hanmandlu et al., 2003] Hanmandlu, M., Jha, D., and Sharma, R. (2003). Color image enhancement by fuzzy intensification. *Pattern Recognition Letters*, 24(1-3):81–87.

[Hashemi et al., 2010] Hashemi, S., Kiani, S., Noroozi, N., and Moghaddam, M. E. (2010). An image contrast enhancement method based on genetic algorithm. *Pattern Recognition Letters*, 31(13):1816–1824.

[Horng, 2011] Horng, M.-H. (2011). Multilevel thresholding selection based on the artificial bee colony algorithm for image segmentation. *Expert Systems with Applications*, 38(11):13785 – 13791.

[Jin and Yang, 2011] Jin, Z. and Yang, X. (2011). A variational model to remove the multiplicative noise in ultrasound images. *Journal of Mathematical Imaging and Vision*, 39(1):62–74.

[Kao et al., 2010] Kao, W.-C., Hsu, M.-C., and Yang, Y.-Y. (2010). Local contrast enhancement and adaptive feature extraction for illumination-invariant face recognition. *Pattern Recognition*, 43(5):1736–1747.

[Kim and Cho, 2006] Kim, K.-J. and Cho, S.-B. (2006). A comprehensive overview of the applications of artificial life. *Artificial Life*, 12(1):153–182.

[Lai et al., 2012] Lai, Y.-R., Chung, K.-L., Lin, G.-Y., and Chen, C.-H. (2012). Gaussian mixture modeling of histograms for contrast enhancement. *Expert Systems with Applications*, 39(8):6720 – 6728.

[Ma et al., 2010a] Ma, Z., Jorge, R. N. M., and ao Manuel R. S. Tavares, J. (2010a). A shape guided c-v model to segment the levator ani muscle in axial magnetic resonance images. *Medical Engineering & Physics*, 32(7):766–774.

[Ma et al., 2010b] Ma, Z., Tavares, J. M. R., Jorge, R. N., and Mascarenhas, T. (2010b). A review of algorithms for medical image segmentation and their applications to the female pelvic cavity. *Computer Methods in Biomechanics and Biomedical Engineering*, 13(2):235–246.

[McInerney et al., 2002] McInerney, T., Hamarneh, G., Shenton, M., and Terzopoulos, D. (2002). Deformable organisms for automatic medical image analysis. *Medical Image Analysis*, 6(3):251–266.

[Nguyen and Ranganath, 2012] Nguyen, T. D. and Ranganath, S. (2012). Facial expressions in american sign language: Tracking and recognition. *Pattern Recognition*, 45(5):1877–1891.

[Nomura et al., 2005] Nomura, S., Yamanaka, K., Katai, O., Kawakami, H., and Shiose, T. (2005). A novel adaptive morphological approach for degraded character image segmentation. *Pattern Recognition*, 38(11):1961–1975.

[Oliveira et al., 2010] Oliveira, F. P., Pataky, T. C., and Tavares, J. M. R. (2010). Registration of pedobarographic image data in the frequency domain. *Computer Methods in Biomechanics and Biomedical Engineering*, 3(6):731–740.

[Oliveira et al., 2011] Oliveira, F. P. M., Sousa, A., Santos, R., and Tavares, J. M. R. S. (2011). Spatio-temporal alignment of pedobarographic image sequences. *Medical and Biological Engineering and Computing*, 49(7):843–850.

[Osuna-Enciso et al., 2013] Osuna-Enciso, V., Cuevas, E., and Sossa, H. (2013). A comparison of nature inspired algorithms for multi-threshold imagesegmentation. *Expert Systems with Applications*, 40(4):1213 – 1219.

[Papa et al., 2012] Papa, J. a. P., Falcão, A. X., de Albuquerque, V. H. C., and Tavares, J. a. M. R. S. (2012). Efficient supervised optimum-path forest classification for large datasets. *Pattern Recognition*, 45(1):512–520.

[Peter et al., 2008] Peter, Z., Bousson, V., Bergot, C., and Peyrin, F. (2008). A constrained region growing approach based on watershed for the segmentation of low contrast structures in bone micro-ct images. *Pattern Recognition*, 41(7):2358–2368.

[Petersen et al., 2002] Petersen, E. M., Deridder, D., and Handels, H. (2002). Image processing with neural networks - a review. *Pattern Recognition*, 35(10):2279–2301.

[Pinho and Tavares, 2009] Pinho, R. R. and Tavares, J. M. R. (2009). Tracking features in image sequences with kalman filtering, global optimization, mahalanobis distance and a management model. *Computer Modeling in Engineering & Sciences*, 46(1):55–75.

[Prasad et al., 2011a] Prasad, G., Joshi, A. A., Feng, A., Barysheva, M., Mcmahon, K. L., De Zubicaray, G. I., Martin, N. G., Wright, M. J., Toga, A. W., Terzopoulos, D., and Thompson, P. M. (2011a). Deformable Organisms and Error Learning for Brain Segmentation. In Pennec, X., Joshi, S., and Nielsen, M., editors, *Proceedings of the Third International Workshop on*

Mathematical Foundations of Computational Anatomy - Geometrical and Statistical Methods for Modelling Biological Shape Variability, pages 135–147.

[Prasad et al., 2011b] Prasad, G., Joshi, A. A., Thompson, P. M., Toga, A. W., Shattuck, D. W., and Terzopoulos, D. (2011b). Skull-stripping with deformable organisms. In *ISBI'11*, pages 1662–1665.

[Ramponi et al., 1996] Ramponi, G., Strobel, N. K., Mitra, S. K., and Yu, T.-H. (1996). Nonlinear unsharp masking methods for image contrast enhancement. *Journal of Electronic Imaging*, 5(3):353–367.

[Shkvarko et al., 2011] Shkvarko, Y., Atoche, A. C., and Torres-Roman, D. (2011). Near real time enhancement of geospatial imagery via systolic implementation of neural network-adapted convex regularization techniques. *Pattern Recognition Letters*, 32(16):2197–2205.

[Srinivasan and Sundaram, 2013] Srinivasan, A. and Sundaram, S. (2013). Applications of deformable models for in-dopth analysis and feature extraction from medical images–a review. *Pattern Recognition and Image Analysis*, 23(2):296–318.

[Terzopoulos, 1999] Terzopoulos, D. (1999). Artificial life for computer graphics. *Communications of the ACM*, 42(8):32–42.

[Trifas et al., 2006] Trifas, M. A., Tyler, J. M., and Pianykh, O. S. (2006). Applying multiresolution methods to medical image enhancement. In *Proceedings of the 44th annual Southeast regional conference*, ACM-SE 44, pages 254–259, New York, NY, USA. ACM.

[Wang and Tan, 2011] Wang, J. and Tan, Y. (2011). Morphological image enhancement procedure design by using genetic programming. In *Proceedings of the 13th annual conference on Genetic and evolutionary computation*, GECCO '11, pages 1435–1442, New York, NY, USA. ACM.

[Wang et al., 2002] Wang, Z., Bovik, A. C., and Lu, L. (2002). Why is image quality assessment so difficult? In *Proceedings of IEEE International Conference on Acoustic, Speech, and Signal Processing*, volume 4.

[Wang et al., 2004] Wang, Z., Bovik, A. C., Sheikh, H. R., and Simoncelli, E. P. (2004). Image quality assessment: from error visibility to structural similarity. *IEEE Transactions on Image Processing*, 13(4):600–612.

[Xue et al., 2003] Xue, J.-H., Pizurica, A., Philips, W., Kerre, E., Van De Walle, R., and Lemahieu, I. (2003). An integrated method of adaptive enhancement for unsupervised segmentation of mri brain images. *Pattern Recognition Letters*, 24(15):2549–2560.

[Yang et al., 2009] Yang, J., Wang, Y., Xu, W., and Dai, Q. (2009). Image and video denoising using adaptative dual-tree discrete wavelet packets. *IEEE Transactions on Circuits and Systems for Video Technology*, 19(5):642–655.

[Yi Kim and Jung, 2005] Yi Kim, E. and Jung, K. (2005). Genetic algorithms for video segmentation. *Pattern Recognition*, 38(1):59–73.

[Yu et al., 2010] Yu, J., Tan, J., and Wang, Y. (2010). Ultrasound speckle reduction by a susan-controlled anisotropic diffusion method. *Pattern Recognition*, 43(9):3083–3092.

[Zhang et al., 2010a] Zhang, L., Dong, W., Zhang, D., and Shi, G. (2010a). Two-stage image denoising by principal component analysis with local pixel grouping. *Pattern Recognition*, 43(4):1531–1549.

[Zhang et al., 2010b] Zhang, L., Dong, W., Zhang, D., and Shi, G. (2010b). Two-stage image denoising by principal component analysis with local pixel grouping. *Journal of Pattern Recognition*, 43(4):1531–1549.

FIGURE CAPTIONS

Figure 1: Pyramid usually adopted to create an artificial life model (adapted from [Terzopoulos, 1999]).

Figure 2: Flow diagram of the proposed image enhancement method.

Figure 3: Graph for intensity reduction function for $k = 255$.

Figure 4: Graph of food's height loss due to the degradation caused by the organism and food's high gain due to the growing of the food over time.

Figure 5: Results of the enhancement methods on synthetic images I: (a) original image, (b) affected image with the addition of noise and blurring; images returned after the applying the methods (c) square root enhancement, (d) quadratic enhancement (e) logarithmic enhancement, (f) normalization, (g) histogram equalization and (h) using our method based on a new artificial life model. (The images (a-), (b-), (c-), (d-), (e-), (f-) (g-) and (h-) represent the difference between the respective processed and original images.)

Figure 6: Results of the enhancement methods on syntetic images II: (a) original image, (b) affected image with the addition of noise and blurring; images returned after the applying the methods (c) square root enhancement, (d) quadratic enhancement (e) logarithmic enhancement, (f) normalization, (g) histogram equalization and (h) using our method based on a new artificial life model. (The images (a-), (b-), (c-), (d-), (e-), (f-) (g-) and (h-) represent the difference between the respective processed and original images.)

Figure 7: Results of the enhancement methods on synthetic images III: (a) original image, (b) affected image with the addition of noise and blurring; images returned after the applying the methods (c) square root enhancement, (d) quadratic enhancement (e) logarithmic enhancement, (f) normalization, (g) histogram equalization and (h) using our method based on a new artificial life model. (The images (a-), (b-), (c-), (d-), (e-), (f-) (g-) and (h-) represent the difference between the respective processed and original images.)

Figure 8: Results of the enhancement methods on real images: (a) original image, (b) affected image with the addition of noise and blurring; images returned after the applying the methods (c) square root enhancement, (d) quadratic enhancement (e) logarithmic enhancement, (f) normalization, (g) histogram equalization and (h) using our method based on a new artificial life model.

Figure 9: PSNR graph plotted from the data in Table 1.

Figure 10: SSIM graph plotted from the data in Table 2.

Figure 11: Profile of the 128th line (randomly chosen) of the original images, affected images, and image returned from our method applied on the images of Figures 5, 6 and 7.

Figure 12: Representation of the points classified as belonging to the class DV marked in black: (a) original image, (b) damaged image with the addition of noise and blurring operations; images after application of the (c) square root enhancement method, (d) quadratic enhancement method, (e) logarithmic enhancement method, (f) normalization, (g) histogram equalization, and (h) using our method based on a new artificial life model.

Figure 13: Results of the enhancement methods on real images: the original image (a), original image segmented (b), segmentation of images returned by the square root enhancement method (c), quadratic enhancement method, (d) logarithmic enhancement method (e), normalization (f), histogram equalization (g), and the proposed enhancement method (h).

TABLE CAPTIONS

Table 1: PSNR indexes of the proposed method and other methods for image enhancement presented in the literature. (The lines with values in bold are related to the images of Figs. 5-7.)

Table 2: SSIM indexes of the proposed method and other methods for image enhancement presented in the literature. (The lines with values in bold are related to the images of Figs. 5-7.)

Table 3: DV and BV values for the images of Figure 8. (The values indicated in bold are the ones that should be approximated.)

Table 4: Computational times (in ms) to enhance the images "Lena" and "Cameramen".

TABLES

Table 1

Image	Affected Image	Histogram Equalization	Normalization	Quadratic Enhancement	Square Root Enhancement	Logarithmic Enhancement	Proposed Method
1	**5.780**	**1.327**	**4.312**	**1.553**	**9.787**	**10.402**	**12.457**
2	5.009	1.406	4.462	2.218	7.794	10.936	12.930
3	3.602	1.716	3.083	1.644	7.597	9.723	12.020
4	**9.090**	**0.455**	**6.640**	**2.635**	**17.130**	**14.151**	**18.394**
5	5.791	1.348	4.353	1.571	10.392	10.671	15.153
6	4.952	1.326	4.240	2.236	7.990	11.558	15.337
7	**3.698**	**1.666**	**2.693**	**1.667**	**8.220**	**10.398**	**16.091**
8	8.892	0.443	6.220	2.650	16.543	14.244	18.307
9	6.156	0.946	4.210	2.261	9.787	10.183	12.191
10	4.731	1.560	2.538	2.103	6.951	6.891	8.215
11	4.813	1.479	4.109	2.099	6.241	7.025	8.388
12	4.106	2.260	3.690	3.781	4.856	4.878	5.628
13	6.351	1.024	4.176	2.191	10.978	10.202	13.726
14	5.090	1.522	2.641	2.111	7.910	6.891	9.473
15	4.959	1.427	3.595	2.109	7.142	7.148	10.004
16	5.018	2.202	4.451	4.222	5.235	4.885	6.397

Table 2

Image	Affected Image	Histogram Equalization	Normalization	Quadratic Enhancement	Square Root Enhancement	Logarithmic Enhancement	Proposed Method
1	**0.147**	**0.078**	**0.103**	**0.061**	**0.597**	**0.578**	**0.728**
2	0.265	0.059	0.234	0.113	0.559	0.597	0.747
3	0.134	0.091	0.127	0.120	0.435	0.533	0.722
4	**0.448**	**0.011**	**0.338**	**0.113**	**0.884**	**0.828**	**0.917**
5	0.169	0.092	0.127	0.078	0.631	0.601	0.844
6	0.272	0.060	0.240	0.118	0.610	0.637	0.843
7	**0.162**	**0.100**	**0.136**	**0.129**	**0.536**	**0.598**	**0.874**
8	0.440	0.012	0.324	0.127	0.871	0.829	0.912
9	0.308	0.039	0.199	0.033	0.654	0.666	0.765
10	0.133	0.025	0.073	0.060	0.376	0.412	0.536
11	0.195	0.007	0.126	0.012	0.418	0.482	0.560
12	0.100	0.022	0.116	0.135	0.168	0.208	0.268
13	0.337	0.070	0.197	0.044	0.700	0.667	0.814
14	0.185	0.025	0.094	0.071	0.439	0.412	0.603
15	0.224	0.024	0.117	0.026	0.482	0.498	0.650
16	0.179	0.028	0.190	0.212	0.211	0.210	0.337

Table 3

Image	Original Image		Affected Image		Histogram Equalization		Normalization		Quadratic Enhancement		Square Root Enhancement		Logarithmic Enhancement		Proposed Method	
	DV	BV	DV	BV	DV	BV	DV	BV	DV	BV	DV	BV	DV	BV	DV	BV
Cup	**3.18**	**0.05**	1.41	0.24	5.37	0.30	1.82	0.25	2.21	0.29	1.06	0.15	0.67	0.04	4.48	0.03
Lena	**2.81**	**0.07**	1.34	0.22	5.21	0.26	2.39	0.18	2.62	0.18	0.82	0.18	0.54	0.04	2.65	0.06
Came-ramen	**4.27**	**0.04**	1.63	0.19	5.34	0.24	2.28	0.20	2.81	0.21	1.02	0.13	0.51	0.06	5.47	0.03
Parrot	**2.51**	**0.15**	1.40	0.15	6.29	0.22	1.97	0.13	2.66	0.14	0.92	0.13	0.71	0.03	3.06	0.06

Table 4

Image	Histogram Equalization	Normalization	Quadratic Enhancement	Square Root Enhancement	Logarithmic Enhancement	Proposed Method
Lena	0.11	0.62	5.40	1.35	4.68	1460.05
Cameramen	0.11	0.52	5.41	1.35	4.68	2926.87

FIGURES

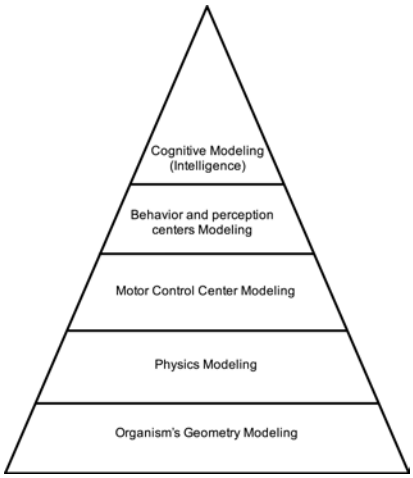

Figure 1

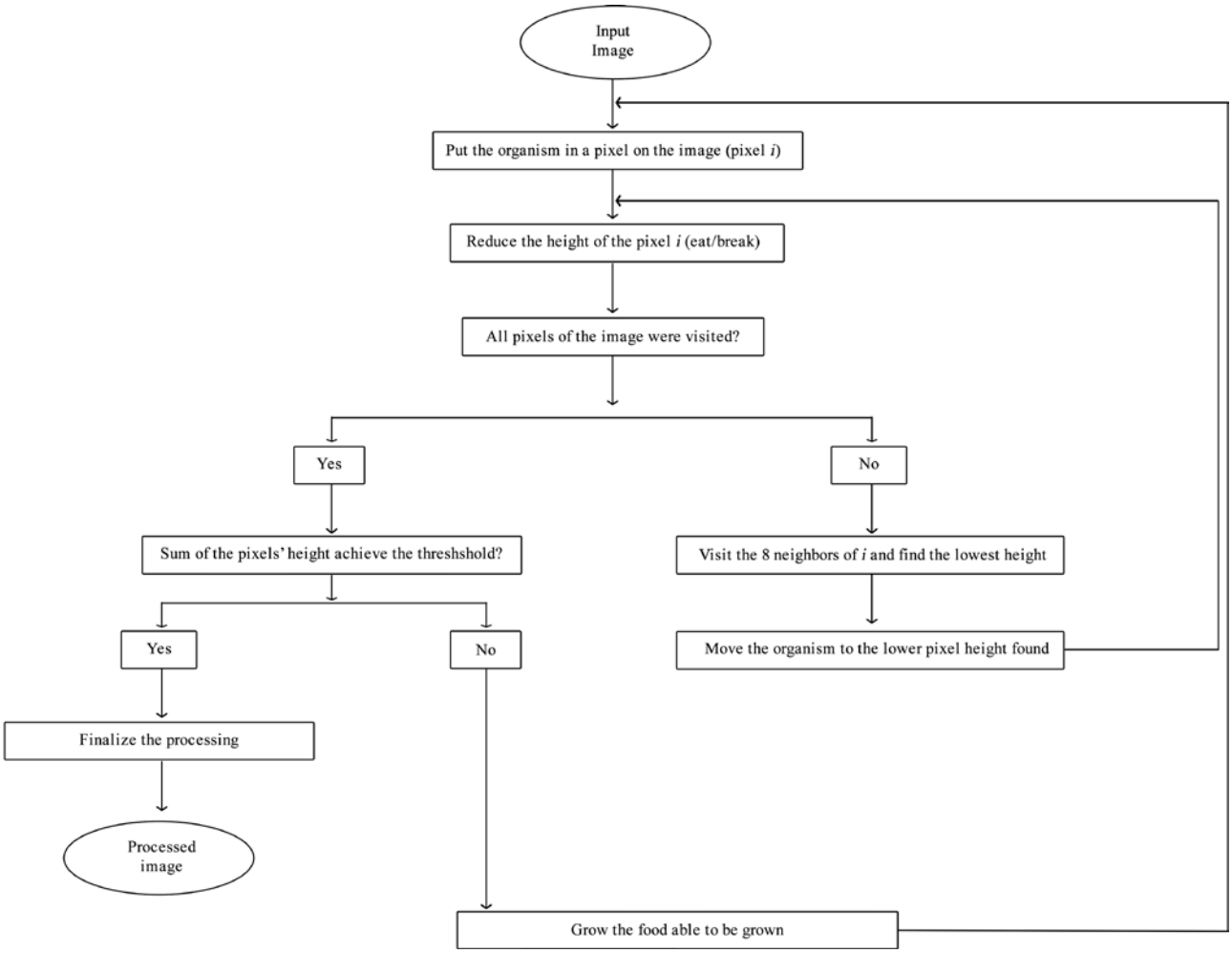

Figure 2

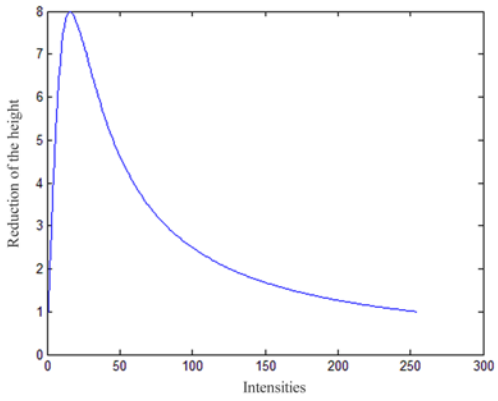

Figure 3

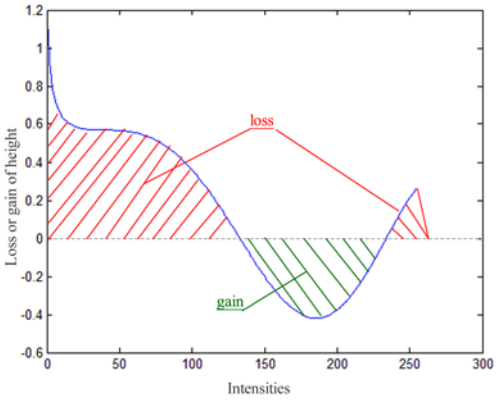

Figure 4

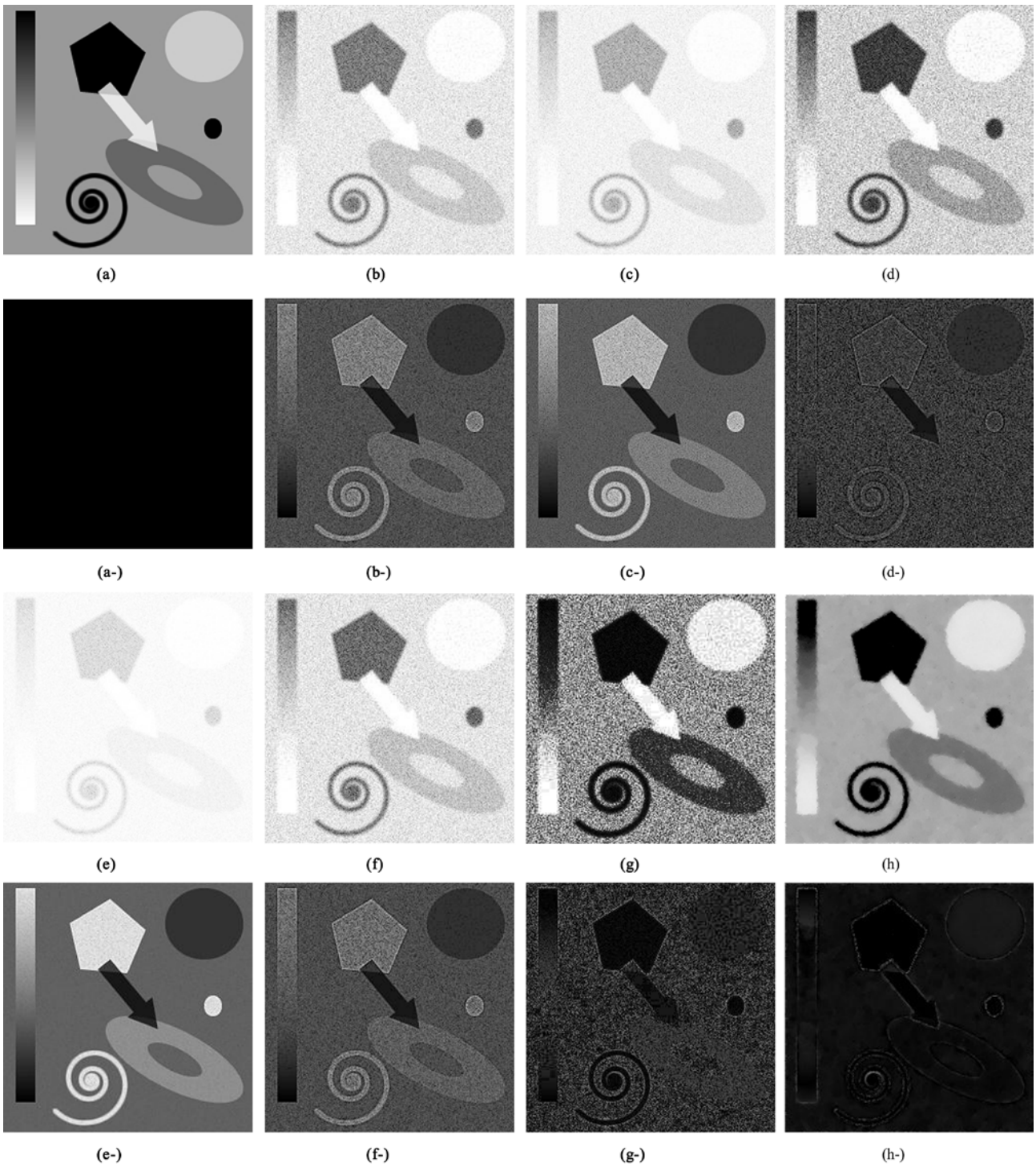

Figure 5

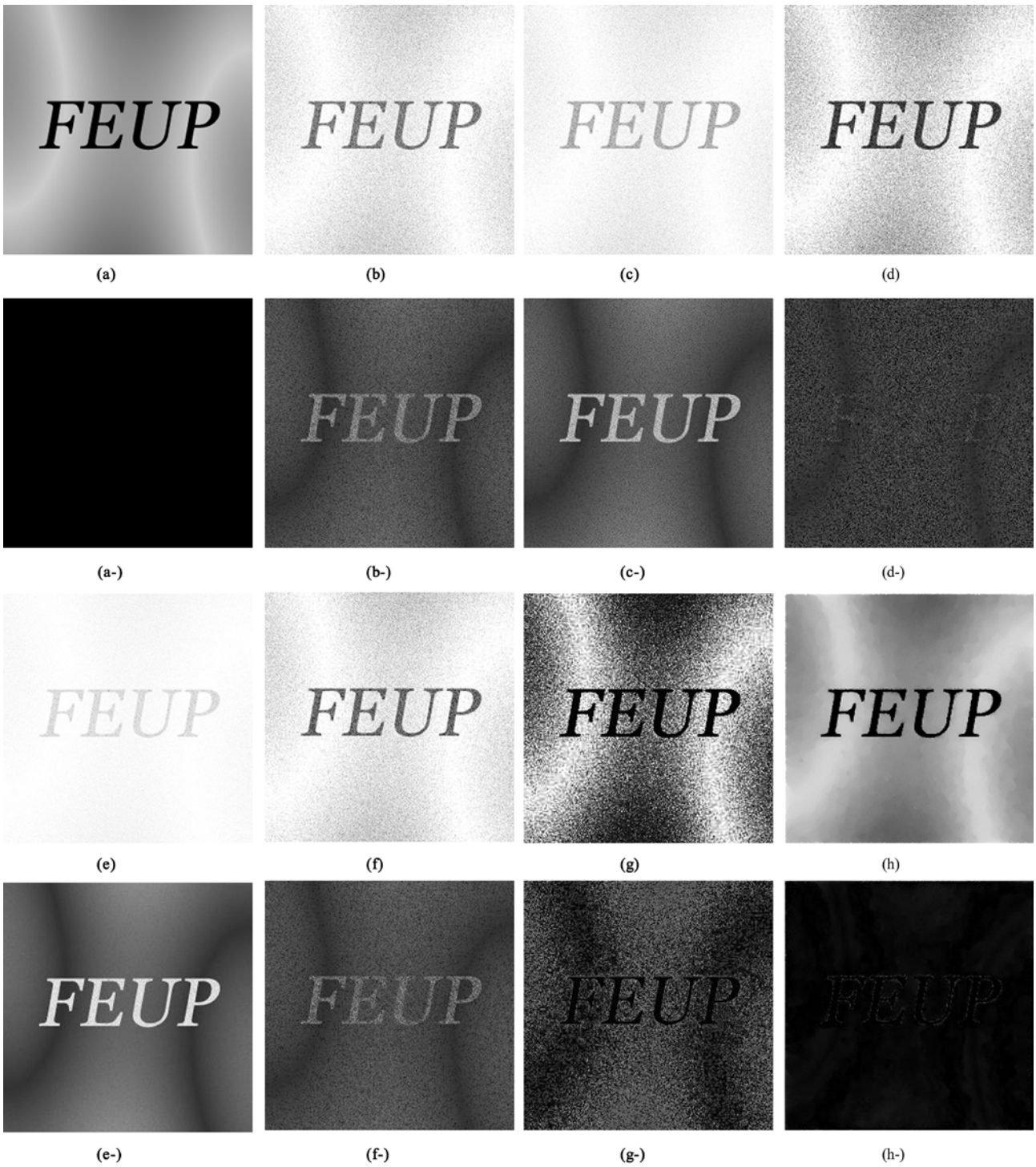

Figure 6

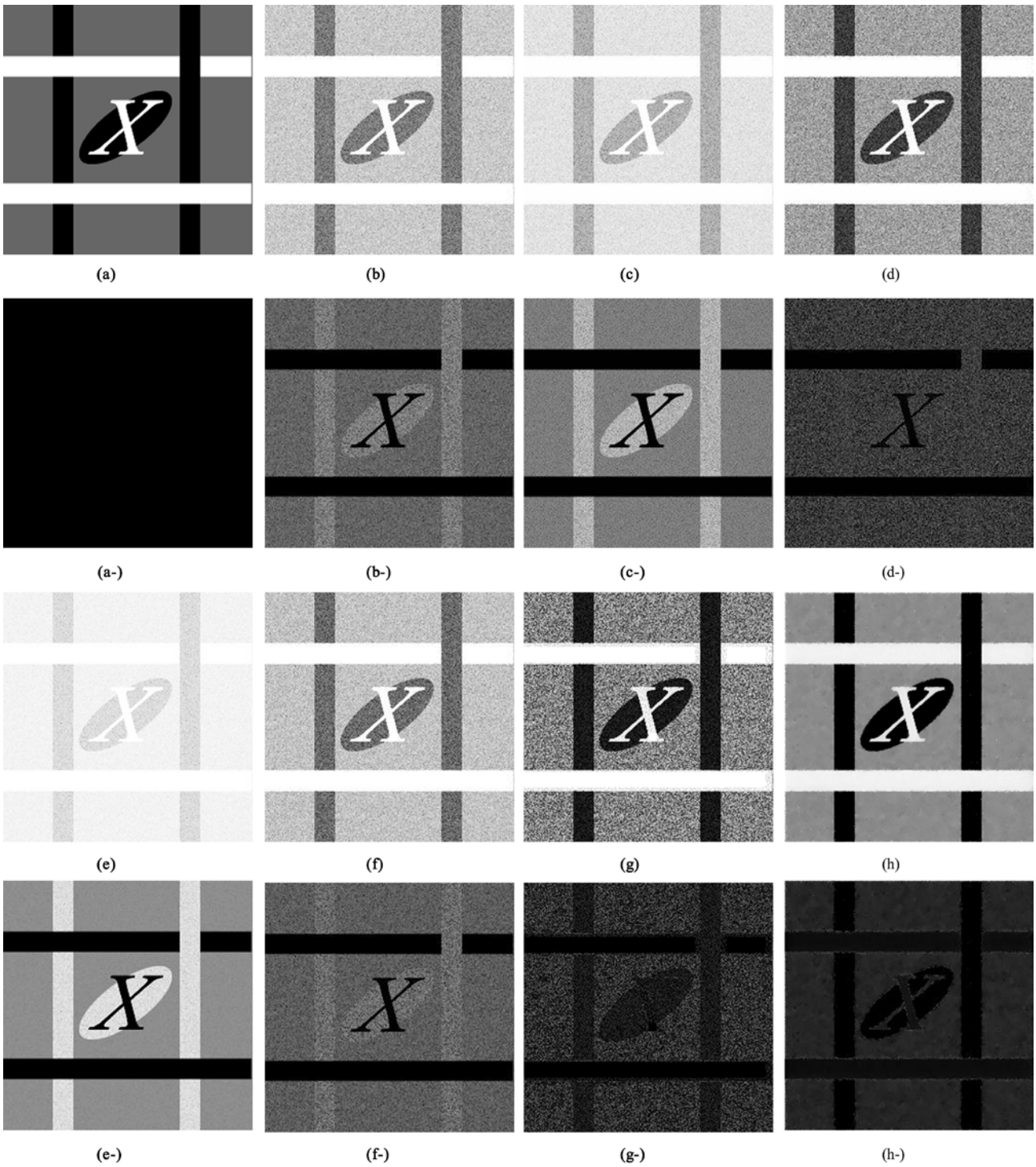

Figure 7

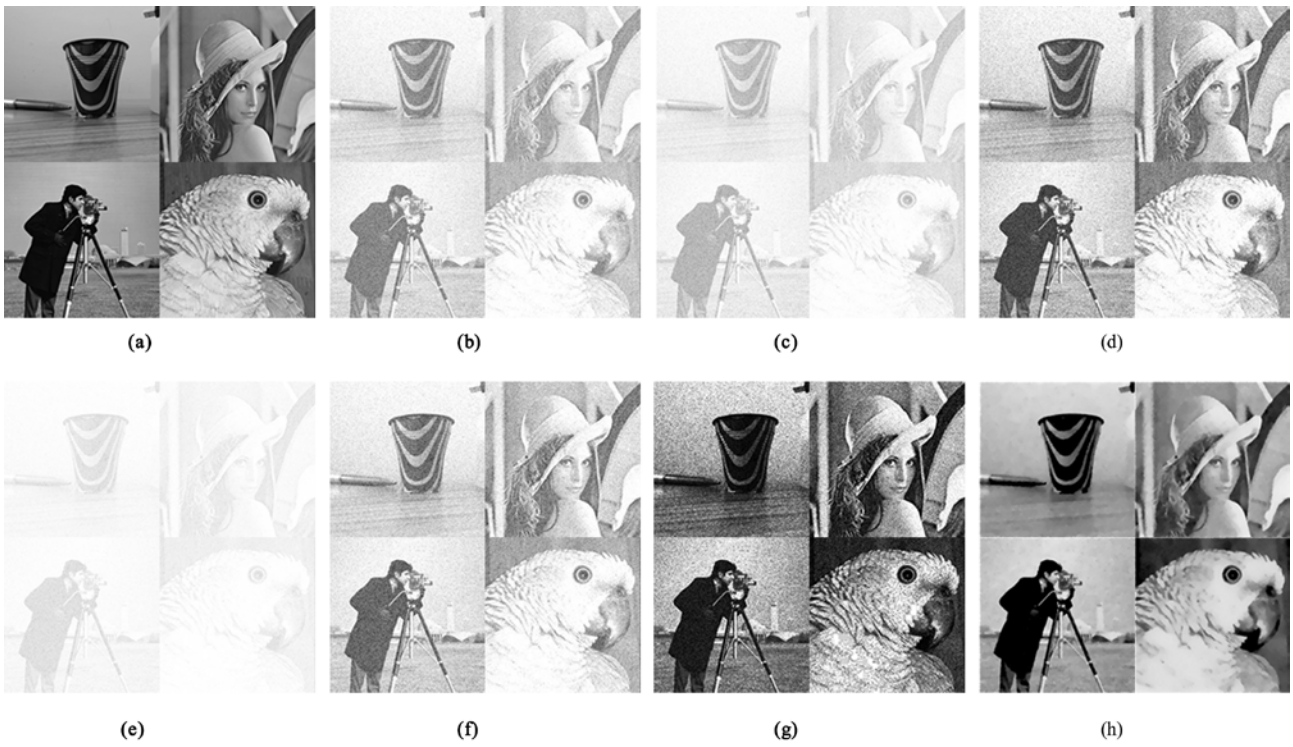

Figure 8

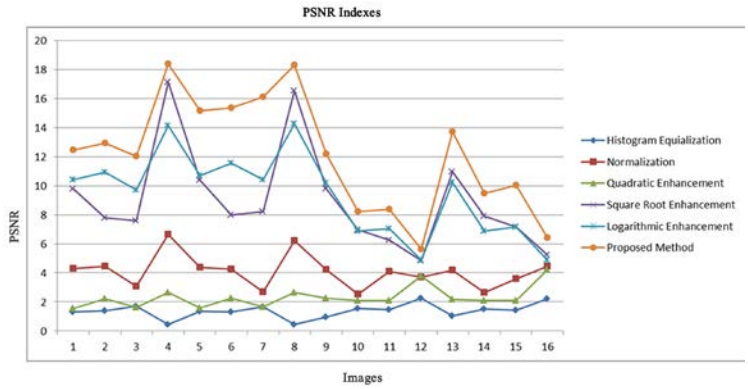

Figure 9

Figure 10

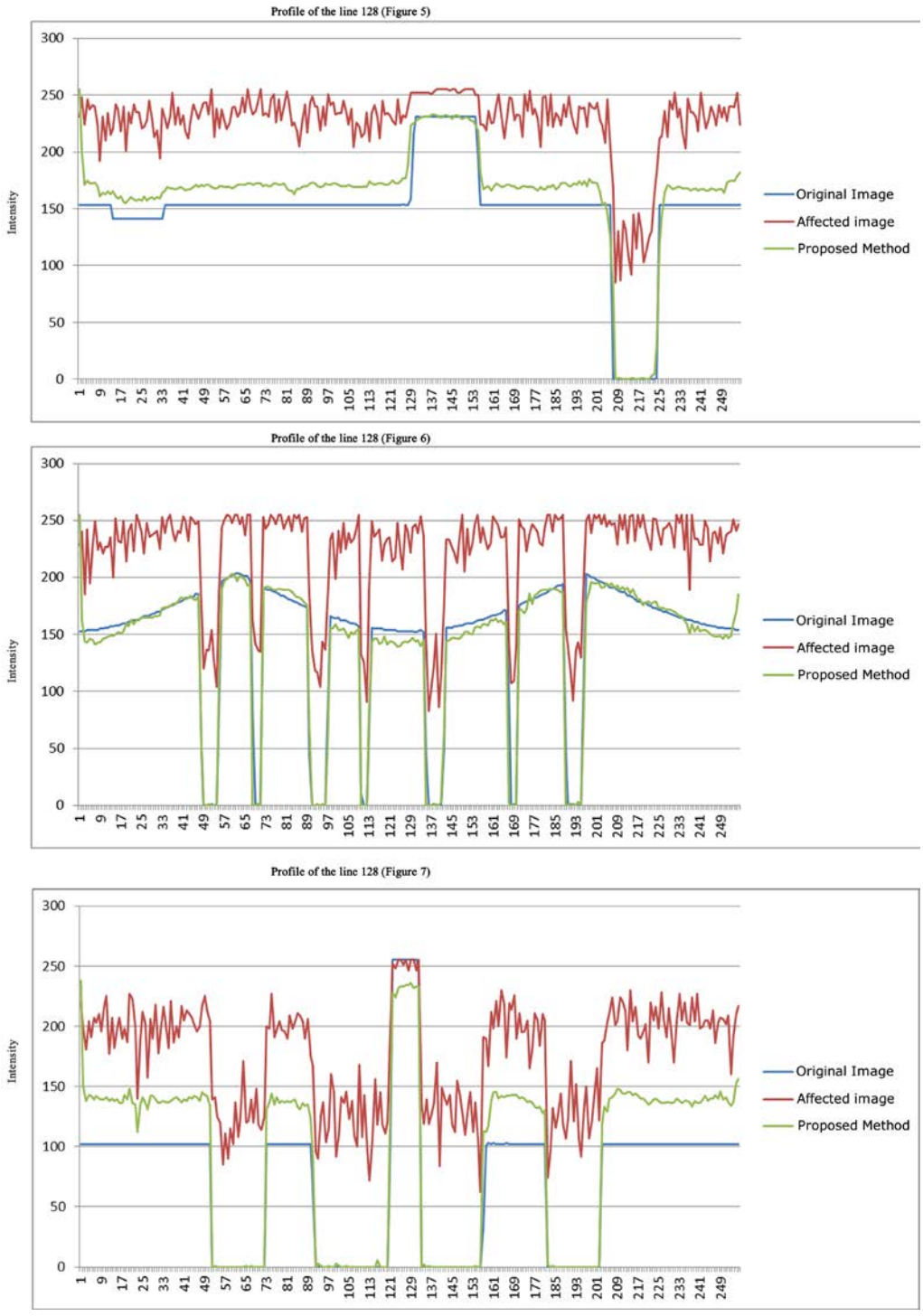
Profile of the line 128 (Figure 5)
Intensity
Original Image
Affected image
Proposed Method
Profile of the line 128 (Figure 6)
Intensity
Original Image
Affected image
Proposed Method
Profile of the line 128 (Figure 7)
Intensity
Original Image
Affected image
Proposed Method

Figure 11

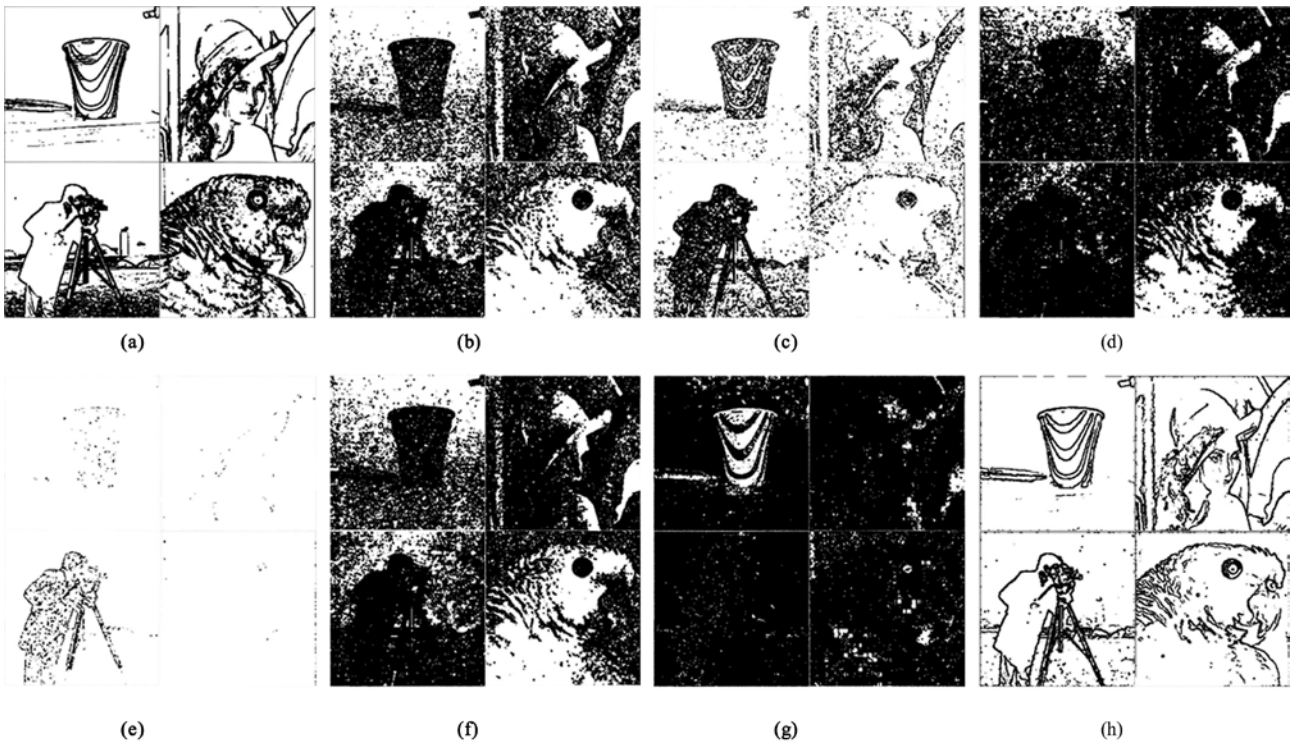

Figure 12

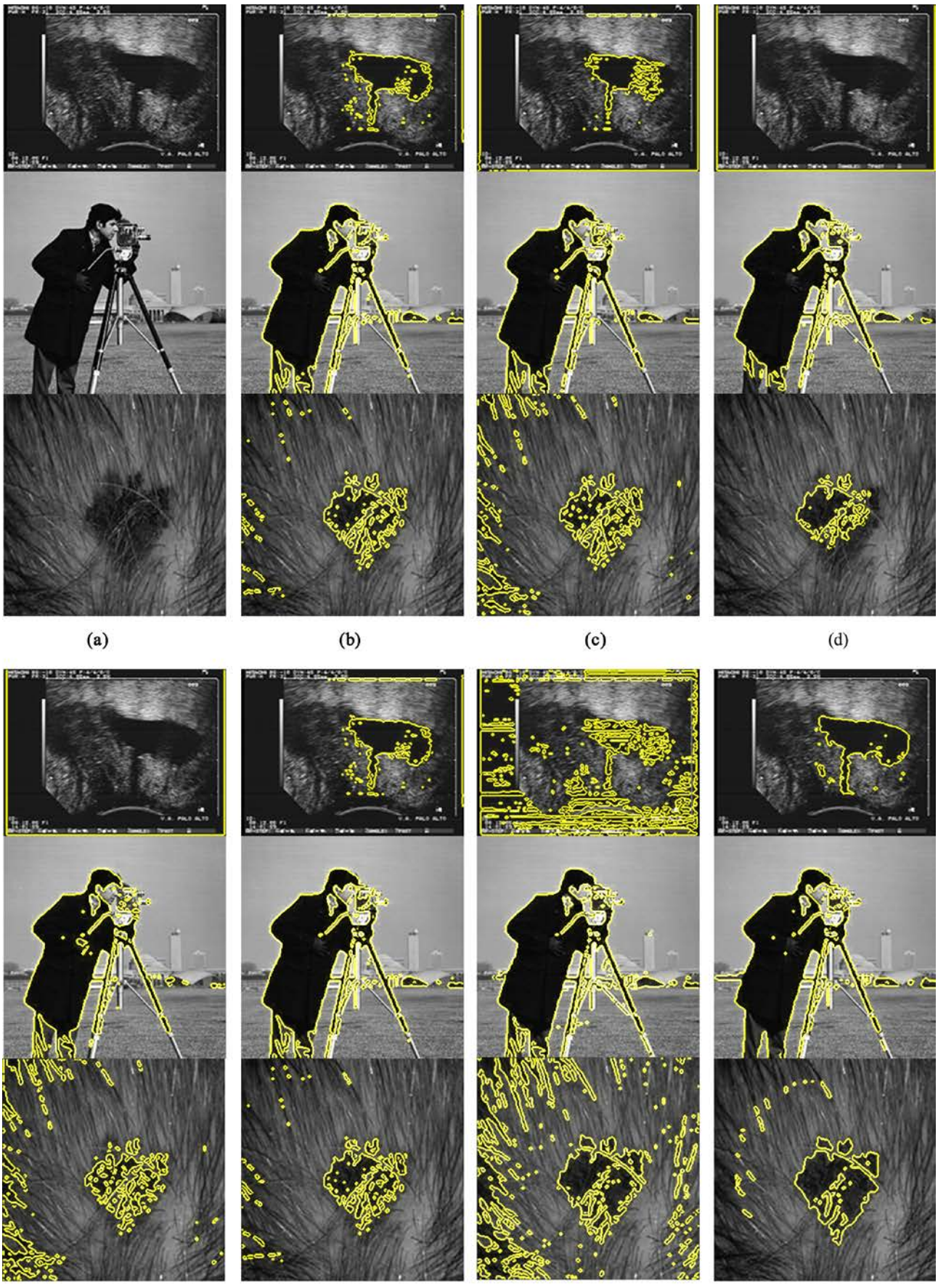

Figure 13